SUPPORTING INFORMATION

PROBING THE DEFECT-DRIVEN TUNABLE PHOTO (ELECTRO) CATALYTIC WATER SPLITTING BEHAVIOR OF PULSED LASER DEPOSITED TITANIA

Jayashree Swaminathan[a]* Subbiah Ravichandran[a]* Parthiban Palani[b], Mahendran Mathankumar[c] and Subramanian Balasubramanian [c]

[a]Electro-inorganic Chemicals Division, CSIR-Central Electrochemical Research Institute, Karaikudi 630003, Tamilnadu, India

[b]Unité de Dynamique et Structure des Matériaux Moléculaires (UDSMM), Université du Littoral Côte d'Opale (ULCO) - CS 80699, F- 62228 Calais cedex – France

[c]Electrochemical Materials Science Division, CSIR-Central Electrochemical Research Institute, Karaikudi 630003, Tamilnadu, India

Selected Area Electron Diffraction (SAED) pattern analysis:

The SAED pattern of PLD-2 and PLD-6 are shown in Fg. S2. As seen, PLD-2 and PLD-6 exhibit spot and ring pattern, respectively. On neglecting the double diffraction spots of PLD-2, we observe the crystal spots along with hkl value of (200), (11-1),(-11-1), (-200), (-1-11) and (1-11) are well matched with the hkl values of anatase phase. While ring pattern of PLD-6 matches with the hexagonal structure and belongs to the crystal family of the tetragonal cuboid with the zone axis of [111]. These results affirm the formation of single crystalline anatase phase in PLD-2, while mixed anatase and tetragonal rutile structure in PLD-6.

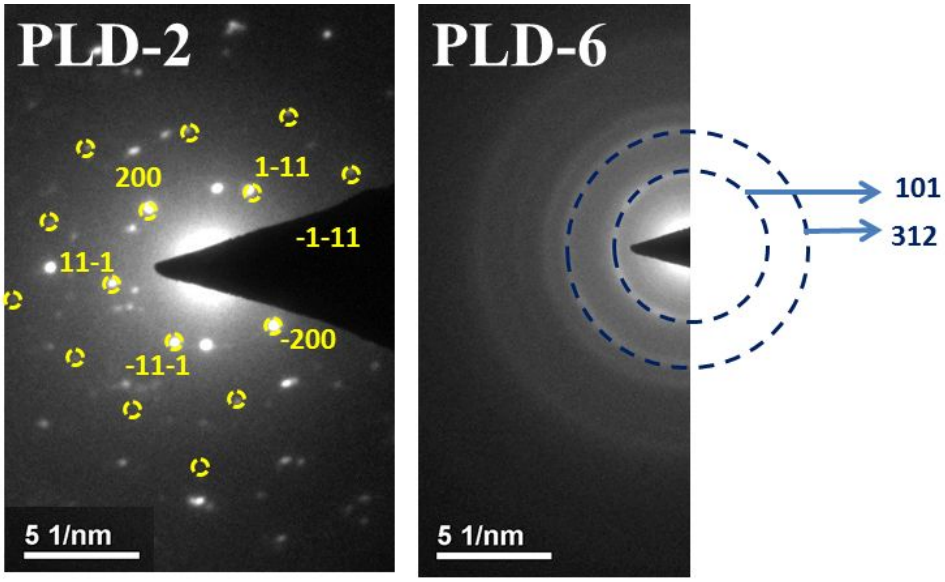

Fig. S1: SAED pattern of PLD-2and PLD-6

XRD pattern analysis:

Table S1 summarizes the refined structural parameters such as variation in unit cell parameter and atomic position in titania with agreement factors.

Sample		Unit cell parameter (Å)			Atomic position					Agreement factors		
		a=b	c	volume	Wyck	x	y	z	Occupancy	Rp	Rwp	Chi^2
PLD-2		3.777 (1)	9.486 (10)	135.35 (7)	4a	0	-0.25	0.125	1	0.45	0.59	6.57
					8f	0	-0.25	0.334	1.275			
PLD-3	A (25.4%)	3.737 (8)	9.315 (6)	130.05 (5)	4a	0	-0.25	0.125	1	0.09	0.21	2.20
					8f	0	-0.25	0.333	0.90			
	R (74.6%)	4.532 (7)	2.957 (5)	60.74 (2)	2a	0	0	0	1			
					4f	0.2961	0.2961	0	0.90			
PLD-4		4.570 (10)	2.947 (6)	61.5 (27)	2a	0	0	0	1	0.18	0.35	1.97
					4f	0.3048	0.3048	0	0.87			
PLD-5		4.574 (5)	2.944 (5)	61.6 (15)	2a	0	0	0	1	0.09	0.21	2.24
					4f	0.3113	0.3113	0	0.85			
PLD-6		4.575 (6)	2.941 (1)	61.5 (16)	2a	0	0	0	1	0.11	0.23	2.57
					4f	0.3313	0.3313	0	0.77			

Table S1: Lattice parameter and atomic position obtained from the Reitveld refinement of the X-ray diffraction data with agreement factors

As seen from Table S1, the decrease in lattice parameter and consequent volume contraction of PLD-3A (oxygen deficient anatase phase) with respect to PLD-2 (oxygen excess anatase phase) is due to rearrangement of Ti-O bonds for rutile phase transformation. On the other hand, the increase in lattice parameter 'a', decrease in lattice parameter 'c' and consequent volume expansion of unit cell of rutile phase with decreasing pO_2 is attributed to combination of reduction in average Ti oxidation state, increase in oxygen vacancy content, weakening (apical distance) and lengthening (quadratic distance) Ti-O bond.[1] This is substantiated by shift of O atomic position in rutile phase towards positive direction of x and y axis in rutile phase with pO_2.

Based on variation in lattice parameter and atomic position of titania with pO_2, we affirm that there is a change in its crystal structure on varying the pO_2. Besides on comparing occupancy of all samples, PLD-2 shows oxygen excess occupancy while all other samples exhibit as oxygen deficient samples. The decreasing oxygen vacancy content with pO_2 confirms that partial pressure in PLD chamber plays a vital role on forming defect-rich titania.

For better understanding, the calculated variation in Ti-O bond length and Ti-O-Ti bond angle of the prepared samples are illustrated in Fig. S2. As seen from Fig. S2, all samples show diverse Ti-O bond length and O-Ti-O bond angle with respect to the ideal value (Bond length: 1.96 A for rutile, 1.95 and 2.01 A for anatase; Bond angles : 90° or 180° for rutile, 77°, 102° and 180° for anatase).[2] This reveals the defect induced structural changes in both phases of titania on varying the pO_2.

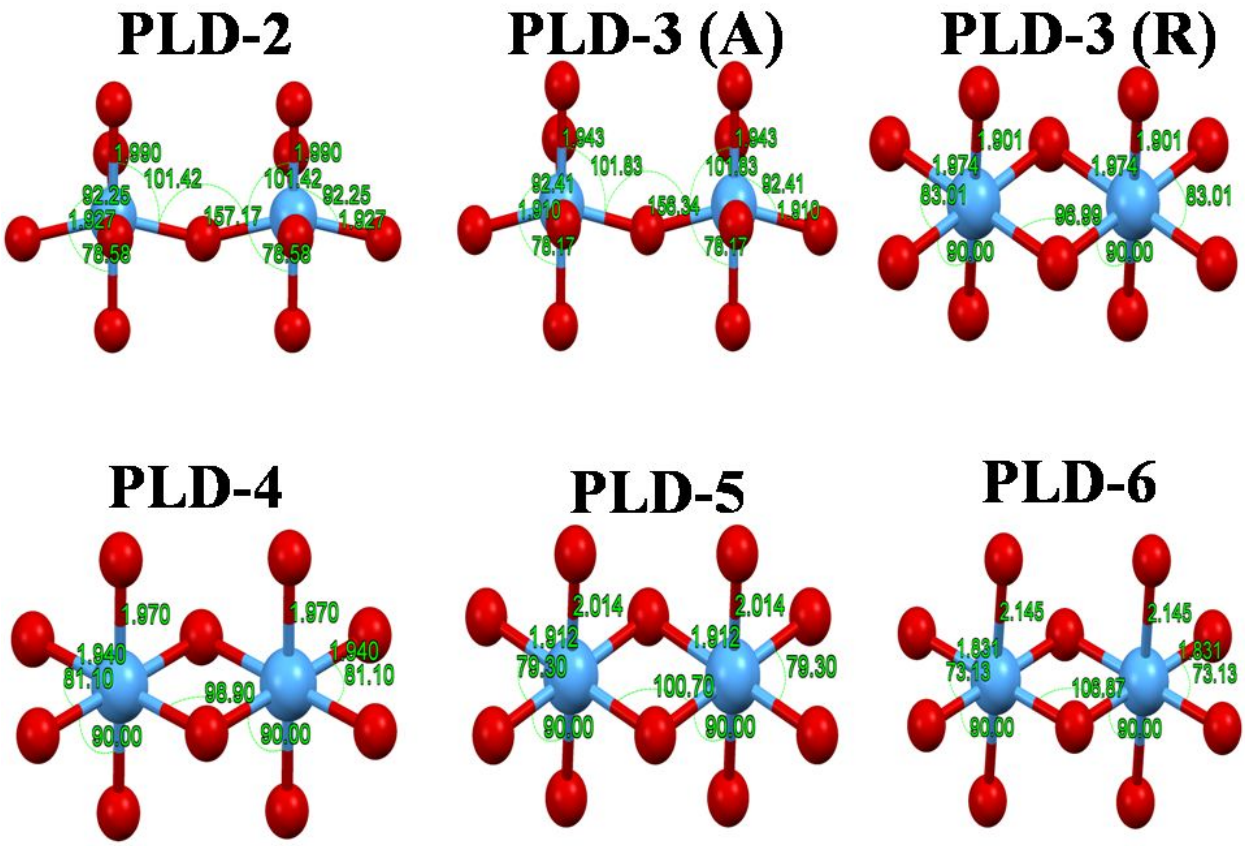

Fig.S2: Representation of Ti -O bond length and Ti-O-Ti bond angle of the prepared samples, where blue and red sphere indicate the Ti and O position

We have also calculated the apical and equatorial Ti-O distance, Ti- Ti interaction and summarized in Table S2.

Sample		PLD-2	PLD-3		PLD-4	PLD-5	PLD-6
			A (25.4%)	R (75.6%)			
Ti–Ti		3.03182(32)	2.99086(21)	2.9574(3)	2.9475 (6)	2.9444(2)	2.9411(7)
Bond length (Å)	Ti–O Apical distance (2×)	1.9903(7)	1.9430(22)	1.97448(12)	1.9706(4)	2.01448(24)	2.14465(28)
	Ti–O Basal distance (4×)	1.9267(5)	1.91004(33)	1.90101(27)	1.93966(18)	1.91214(9)	1.83099(8)

Table S2: Ti-Ti bond length, Ti-O apical and basal distance of the prepared samples obtained from the Reitveld refinement of the X-ray diffraction data

The variant apical and equatorial distance of Ti-O indicates disparate crystal structures are formed at different pO_2. Besides, the enhanced Ti- Ti contraction with decreasing pO_2 indicates the improved interaction between titanium ions due to oxygen vacancy.

XPS analysis:

The XPS survery spectra of PLD-2, PLD-4 and PLD-6 (Fig. S3) show the presence of Ti, O and not any other impurities.

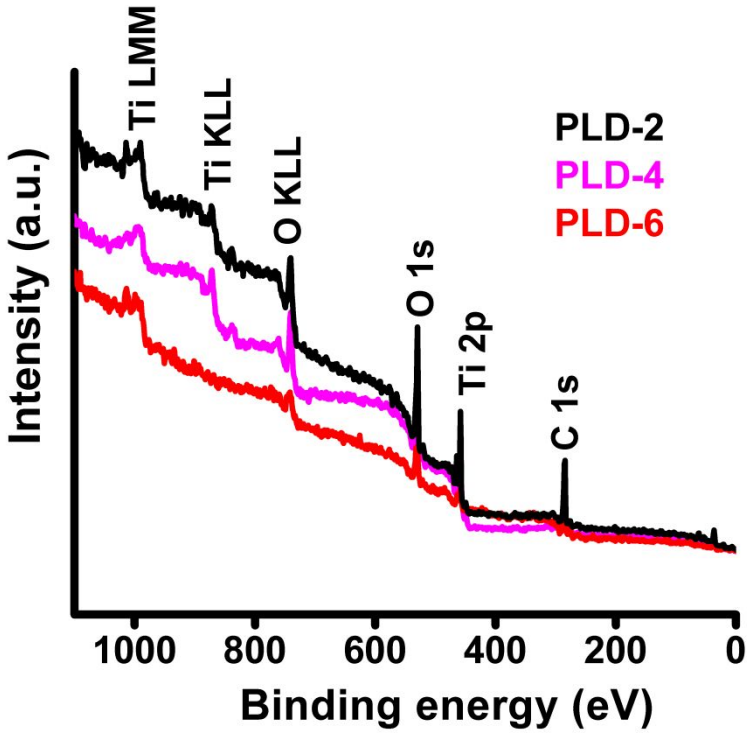

Fig. S3: XPS survey spectra of PLD-2, PLD-4 and PLD-6

In order to know the chemical oxidataion states of PLD-2, PLD-4 and PLD-6, de-convolution of Ti 2p and O 1s have done and shown in Fig. S4. As seen, the de-convoluted Ti 2p spectrum of PLD-2 shows two distinct peaks centered at binding energy of 463.9 eV and 458.1 eV, which are characteristic Ti $2p^{1/2}$ and Ti $2p^{3/2}$ peaks of Ti^{4+}.[3] Besides, high resolution O 1s spectrum of PLD-2 shows peak at 530.08 eV and 532.3 eV, which corresponds to lattice oxygen species (O_L), and chemisorbed OH species (O_{OH}), respectively. [4] This confirms the presence of mere Ti^{4+} ions and surface OH groups in PLD-2. Whereas PLD-4 and PLD-6 exhibit Ti^{3+} ions (B.E. =463.1eV and 457.1 eV)[3] and oxygen vacancy - O_v (B.E. = 531.1 eV), apart from Ti^{4+}, O_L and O_{OH}.[4] The observed negative shift in binding energy (Ti^{3+} and O_v) are accounted for the co-existence of coordinately unsaturated Ti sites and oxygen vacancies in PLD-4 and PLD-6.

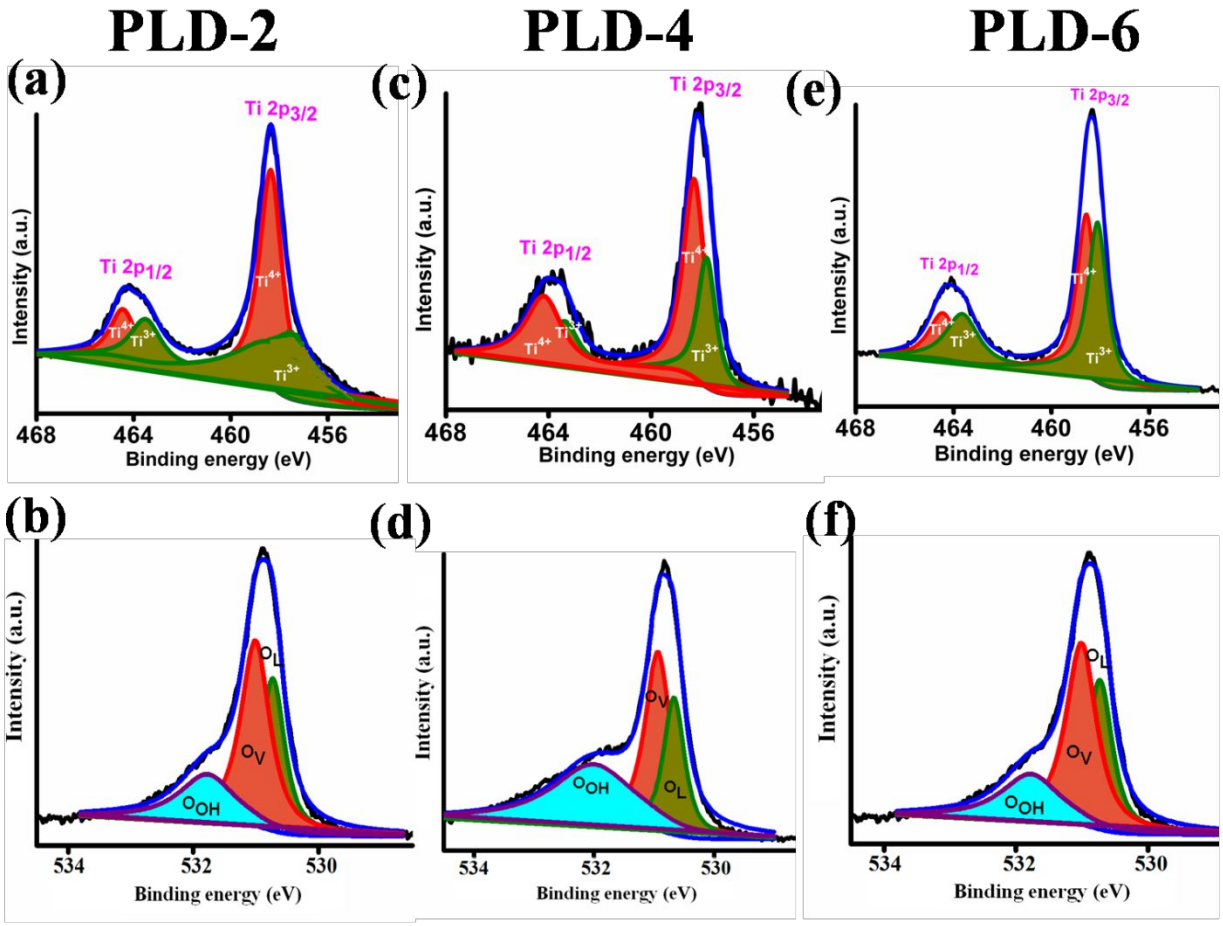

Fig. S4: De-convoluted Ti 2p & O 1s XPS spectra of PLD-2, PLD-4 and PLD-6

Besides, the surface atomic ratio of Ti^{3+}/Ti^{4+} and O/Ti ions in PLD-2, PLD-4 and PLD-6are calculated from areas under the Ti $2p_{3/2,}$ O 1s spectrum of XPS and summarized in Table. S3. As seen, the decreasing ratio of O/Ti and Ti^{4+}/ Ti^{3+} pin-point the profuseness of oxygen vacancies and increased non-stoichiometry in TiO_2 films with decreasing pO_2.

Samples	**Ti^{4+}/ Ti^{3+}**	**O/Ti**
$TiO_{2.40}$	00.67	2.32
$TiO_{1.74}$	0.54	1.84
$TiO_{1.54}$	0	1.63

Table S3: Surface atomic ratio of Ti^{4+} / Ti^{3+} and O/Ti in PLD-2, PLD-4 and PLD-6

FTIR analysis

The functional groups in the prepared samples are analyzed using FTIR spectroscopy and the corresponding FTIR spectra are shown in Fig. S5. Almost all samples exhibit similar absorption features. But on close observation, we inferred the relative variation in broadening and intensity of peaks at different pO_2.

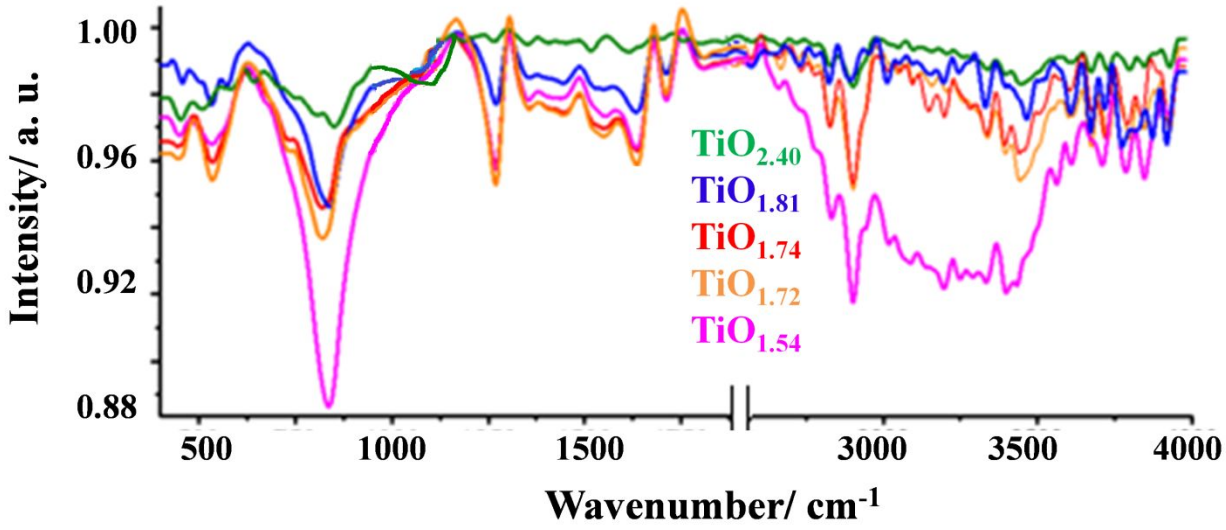

Fig. S5: FTIR spectra of the prepared samples through pulsed laser deposition

The FTIR band around 500-1000 cm^{-1} represents the vibration of Ti-O-Ti bond in titania.[5] These peaks broaden with decreasing pO_2, which indicates more O atom in non- bonding condition in $TiO_{1.54}$ compared to $TiO_{2.40}$. This also illustrates the decrease in Ti-O–Ti bond strength and hence higher Ti−Ti interactions (enhanced oxygen defect density) with decreasing pO_2. Most importantly, formation of interstitial oxygen in $TiO_{2.40}$ is confirmed by the FTIR peak at 1100 cm^{-1}. [6] Besides, the peak around 1400 -1600 cm^{-1} indicates the stretching and bending vibration of Ti-OH group. The FTIR band around 3000- 4000 cm^{-1} represent the incorporation of hydroxyl ion in titania. On particular, the peak at 3488 cm^{-1} is attributed to -OH of titanols located at internal defects sites (where the -O-Ti-O-Ti- chains are interrupted).[7] The peaks at 3400 cm^{-1} represent the stretching modes of free terminal or isolated OH group and fully hydroxylated surface, respectively[8,9]. The peak at 3280 cm^{-1} and 3710 cm^{-1} represent the stretching vibration of internally bound OH group and embedded terminal free OH group, respectively. [28-30] The peaks

at 3716 cm^{-1}, 3685 cm^{-1} and 3640 cm^{-1} represent the stretching vibration of octahedral co-ordinated vacancies (Ti^{3+} - OH^{-}), terminal titanol group -tetrahedral co-ordinated vacancies (Ti^{4+} - OH), and bridging titanol group $(Ti^{4+})_2$– OH, respectively.[18–13] The peak at 3705 cm^{-1} corresponds to titanols (both external and internal sites) [7]. The increasing broadening of 3000-4000 cm^{-1} band with decreasing pO_2 infers the increasing hydroxyl ion incorporation as a result of coordinative unsaturated sites (Ti^{n+}) in titania.

Impedance analysis:

The charge transport kinetics in the prepared samples is studied through impedance spectroscopy and the corresponding nyquist plot is shown in Fig. S6. From the figure, it is clear that transfer of charges is occurred through the diffusion process under dark condition.

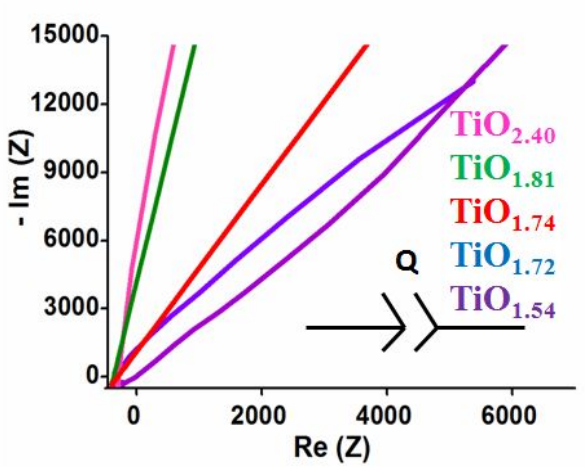

Fig. S6: Nyquist plot of the prepared samples under dark condition

Further, the plot is fitted and obtained equivalent circuit parameters are compared with impedance values under illumination (Table S4). Based on comparison between the values of equivalent circuit elements of the prepared samples with and without illumination, we can infer that there is a variation in kinetics of charge transfer process on illumination.

SAMPLES	EQUIVALENT CIRCUIT ELEMENTS						
	DARK		ILLUMINATION				
	Q_1	a_1	R_s	R_{ct}	Q_2	a_2	Chi^2
$TiO_{2.40}$	$5e^{-5}$	0.701	49.49	524.9	0.421 e-3	0.675	0.123
$TiO_{1.81}$	$5.4e^{-5}$	0.723	68.56	406	$0.640\ e^{-3}$	0.720	0.231
$TiO_{1.74}$	$5.7e^{-5}$	0.795	82.54	2164	$0.835e^{-3}$	0.8217	0.030
$TiO_{1.71}$	$6.5e^{-5}$	0.867	55.89	2914	$0.937e^{-3}$	0.742	0.103
$TiO_{1.54}$	$1e^{-4}$	0.941	46.39	108174	$8.79e^{-2}$	0.983	0.5

Table S4: Calculated equivalent circuit values of the prepared samples through pulsed laser deposition

Mott-Schottky analysis

Mott-Schottky analyses of the prepared samples are done with and without illumination and the corresponding plot is shown in Fig. S7 a & b, respectively. The plot infers the behavioral difference of the sample under dark and light condition. As seen, $TiO_{1.54}$ shows highest donor density and lowest flat-band potential under dark while $TiO_{1.81}$ shows highest donor density and lowest flat-band potential on illumination (Fig. S7 c & d).

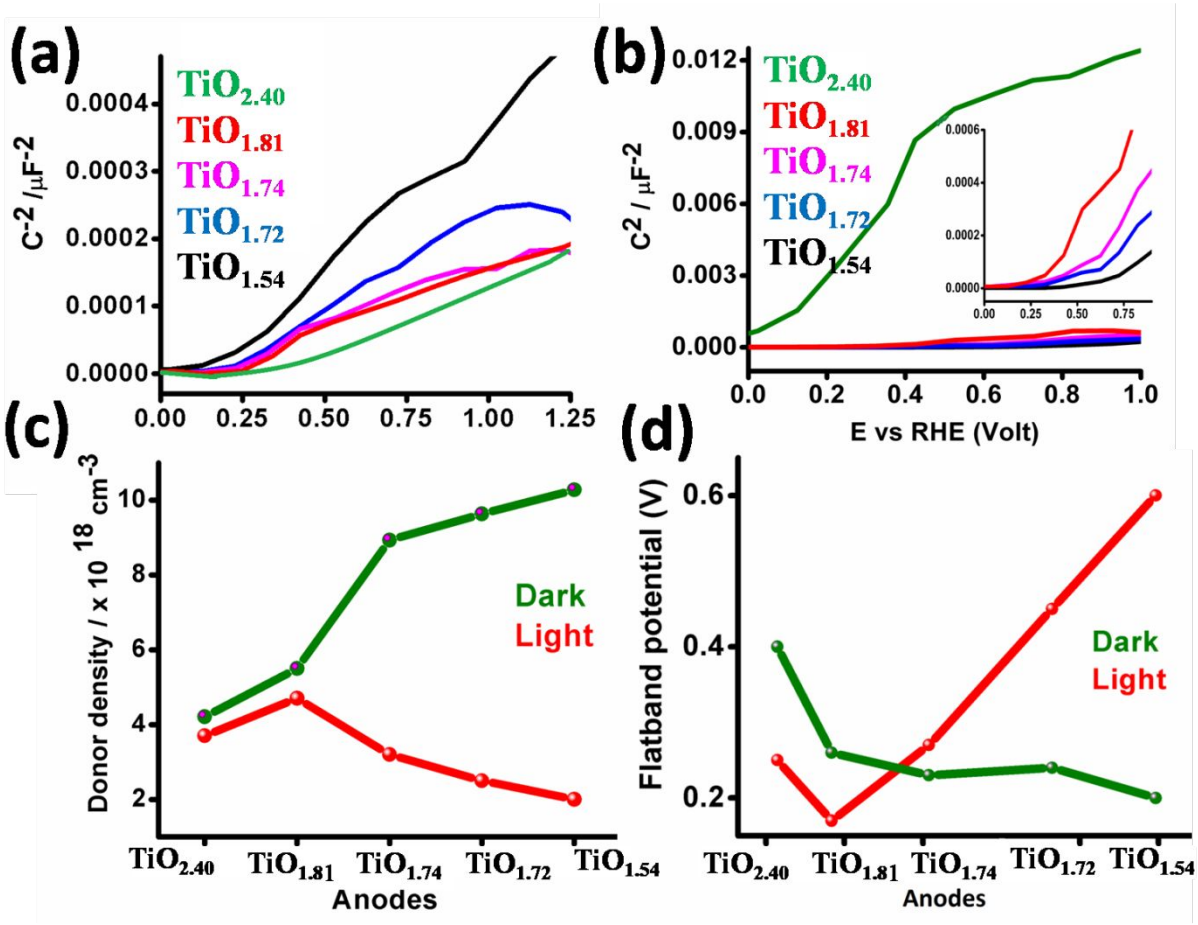

Fig. S7: Mott Schottky plot under (a) dark (b) illumination of the prepared samples; Calculated (c) donor density and (d) flatband potential of the prepared samples

Electron collection time (τ_{IMPS}), electron lifetime (τ_{IMVS}), diffusion length (L_d), charge transfer efficiency (η_{trans}) of the prepared samples:

τ_{IMPS}, τ_{IMVS}, L_d and η_{trans} of the prepared samples are calculated from IMPS and IMVS data and summarized in Fig. S8. As seen, the electron transit time (τ_{IMPS}) is increased with decreasing pO_2 (increasing defect concentration). While, the longest electron lifetime is observed for $TiO_{1.81}$ compared to other samples. This is further substantiated by longer electron diffusion length and higher charge transfer efficiency of $TiO_{1.81}$.

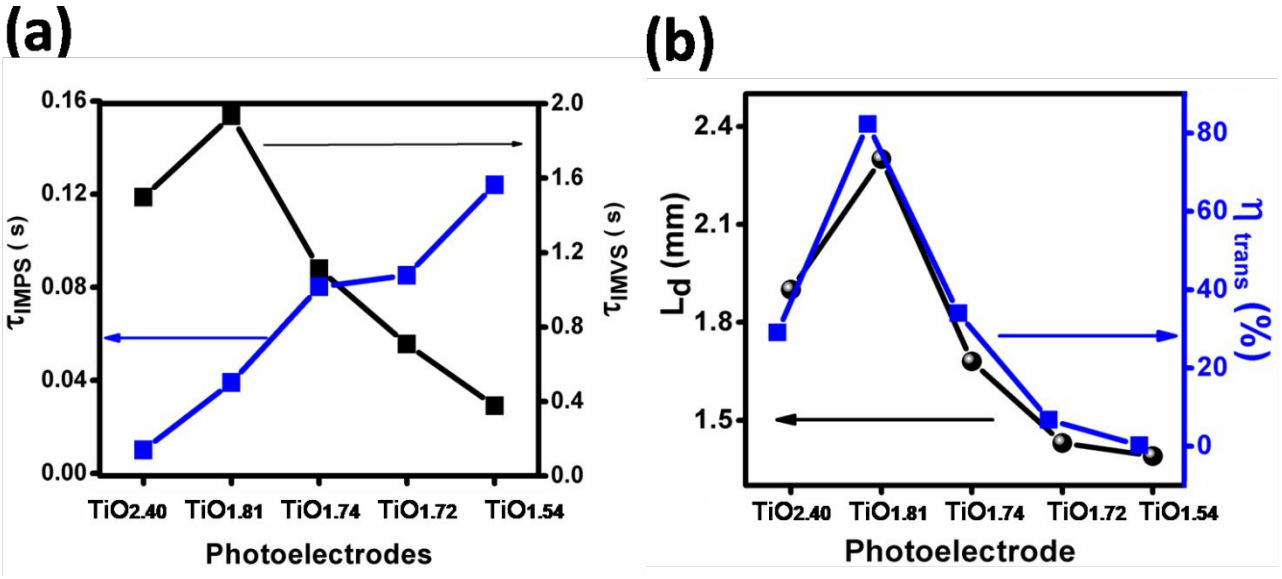

Fig. S8: (a) τ_{IMPS} and τ_{IMVS} (b) L_d and η_{trans} of the prepared samples

Photoluminescence behavior

The photoluminescence emission spectra of the prepared samples at an excitation wavelength of 330 nm are shown in Fig. S9. $TiO_{1.54}$ shows the highest recombination characteristics, followed by $TiO_{1.72}$, $TiO_{1.74,}$ $TiO_{2.40}$ and $TiO_{1.81,}$ respectively. Thus, the less intense PL emission of $TiO_{1.81}$ infers the improved charge transfer at optimum defect content.

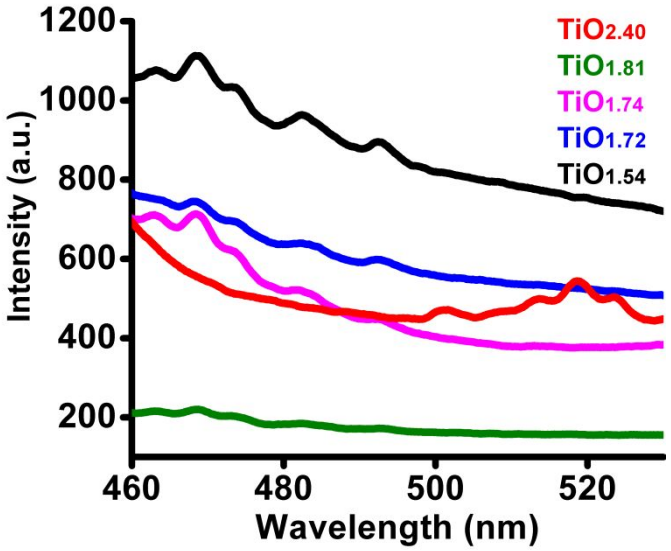

Fig. S9: Photoluminescence spectra of the prepared samples

Analysis of PV decay time

As photovoltage decay rate is inversely proportional to the recombination rate of electron-hole pairs,[14] longer photovoltage decay time of $TiO_{1.81}$ deduces its longer photoelectron lifetime, slower transport with less recombination characteristics (Fig. S10).

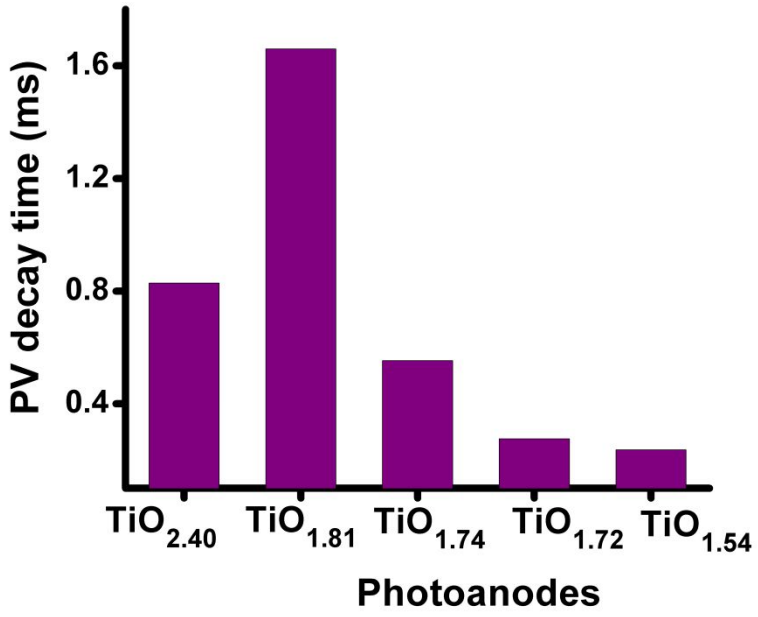

Fig. S10: PV decay time of the prepared samples

References:

1 N. Khatun, S. Tiwari, C. P. Vinod, C. M. Tseng, S. Wei Liu, S. Biring and S. Sen, *J. Appl. Phys.*, , DOI:10.1063/1.5027672.

2 D. Koch and S. Manzhos, *J. Phys. Chem. Lett.*, 2017, **8**, 1593–1598.

3 R. Fu, S. Gao, H. Xu, Q. Wang, Z. Wang, B. Huang and Y. Dai, *RSC Adv.*, 2014, **4**, 37061–37069.

4 M. M. Kumar, S. Badrinarayanan and M. Sastry, *Thin Solid Films*, 2000, **358**, 122–130.

5 R. M. Kadam, B. Rajeswari, A. Sengupta, S. N. Achary, R. J. Kshirsagar and V. Natarajan, *Spectrochim. Acta - Part A Mol. Biomol. Spectrosc.*, 2015, **137**, 363–370.

6 V. Etacheri, M. K. Seery, S. J. Hinder and S. C. Pillai, *Adv. Funct. Mater.*, 2011, **21**, 3744–3752.

7 S. Usseglio, P. Calza, A. Damin, C. Minero, S. Bordiga, C. Lamberti, E. Pelizzetti and A. Zecchina, *Chem. Mater.*, 2006, **18**, 3412–3424.

8 M. Crocker, R. H. M. Herold, A. E. Wilson, M. Mackay, C. a. Emeis and A. M. Hoogendoorn, *J. Chem. Soc. Faraday Trans.*, 1996, **92**, 2791.

9 J. Henych, V. Štengl, A. Mattsson and L. Österlund, *Photochem. Photobiol.*, 2015, **91**, 48–58.

10 A. Ramchiary and S. K. Samdarshi, *Sol. Energy Mater. Sol. Cells*, 2015, **134**, 381–388.

11 Z. Wang, C. Yang, T. Lin, H. Yin, P. Chen, D. Wan, F. Xu, F. Huang, J. Lin, X. Xie and M. Jiang, *Adv. Funct. Mater.*, 2013, **23**, 5444–5450.

12 K. Suriye, R. J. Lobo-Lapidus, G. J. Yeagle, P. Praserthdam, R. D. Britt and B. C. Gates, *Chem. - A Eur. J.*, 2008, **14**, 1402–1414.

13 L. Liu and X. Chen, .

14 X. Gao, D. Guan, J. Huo, J. Chen and C. Yuan, *Nanoscale*, 2013, **5**, 10438–10446.